



# *HST* Detection of Extended Neutral Hydrogen in a Massive Elliptical at $z = 0.4$

Fakhri S. Zahedy<sup>1,2</sup>, Hsiao-Wen Chen<sup>1,3</sup>, Michael Rauch<sup>2</sup>, and Ann Zabludoff<sup>4</sup>

<sup>1</sup>Department of Astronomy & Astrophysics, The University of Chicago, Chicago, IL 60637, USA

<sup>2</sup>The Observatories of the Carnegie Institution for Science, 813 Santa Barbara Street, Pasadena, CA 91101, USA

<sup>3</sup>Kavli Institute for Cosmological Physics, The University of Chicago, Chicago, IL 60637, USA

<sup>4</sup>Department of Astronomy, University of Arizona, Steward Observatory, Tucson, AZ 85721, USA

Received 2017 June 16; revised 2017 August 24; accepted 2017 August 24; published 2017 September 8

## Abstract

We report the first detection of extended neutral hydrogen (H I) gas in the interstellar medium (ISM) of a massive elliptical galaxy beyond  $z \sim 0$ . The observations utilize the doubly lensed images of QSO HE 0047–1756 at  $z_{\text{QSO}} = 1.676$  as absorption-line probes of the ISM in the massive ( $M_{\text{star}} \approx 10^{11} M_{\odot}$ ) elliptical lens at  $z = 0.408$ , detecting gas at projected distances of  $d = 3.3$  and 4.6 kpc on opposite sides of the lens. Using the Space Telescope Imaging Spectrograph, we obtain UV absorption spectra of the lensed QSO and identify a prominent flux discontinuity and associated absorption features matching the Lyman series transitions at  $z = 0.408$  in both sightlines. The H I column density is  $\log N(\text{H I}) = 19.6\text{--}19.7$  at both locations across the lens, comparable to what is seen in 21 cm images of nearby ellipticals. The H I gas kinematics are well-matched with the kinematics of the Fe II absorption complex revealed in ground-based echelle data, displaying a large velocity shear of  $\approx 360 \text{ km s}^{-1}$  across the galaxy. We estimate an ISM Fe abundance of 0.3–0.4 solar at both locations. Including likely dust depletions increases the estimated Fe abundances to solar or supersolar, similar to those of the hot ISM and stars of nearby ellipticals. Assuming 100% covering fraction of this Fe-enriched gas, we infer a total Fe mass of  $M_{\text{cool}}(\text{Fe}) \sim (5\text{--}8) \times 10^4 M_{\odot}$  in the cool ISM of the massive elliptical lens, which is no more than 5% of the total Fe mass observed in the hot ISM.

**Key words:** galaxies: abundances – galaxies: elliptical and lenticular, cD – galaxies: halos – quasars: absorption lines

## 1. Introduction

A large fraction of massive quiescent galaxies are not gas-poor. 21 cm surveys have revealed that 30%–40% of nearby early-type galaxies contain a large amount of neutral hydrogen (H I) gas (e.g., Grossi et al. 2009; Oosterloo et al. 2010; Serra et al. 2012; Young et al. 2014). Beyond the local universe, QSO absorption-line surveys of Mg II  $\lambda\lambda$  2796, 2803 absorption features near luminous red galaxies (LRGs) reveal extended cool gas out to projected distances  $d \gtrsim 100$  kpc, with a mean covering fraction of  $>15\%$  (e.g., Gauthier et al. 2009, 2010; Bowen & Chelouche 2011; Huang et al. 2016). Because Mg II absorption traces photoionized, cool  $T \sim 10^4$  K gas (e.g., Bergeron & Stasińska 1986), the significant covering fraction of Mg II absorbers indicates not only that cool gas is present in these quiescent halos, but also that the gas has been enriched with heavy elements.

The finding that passive galaxies harbor a significant reservoir of chemically enriched cool gas remains a central puzzle in galaxy evolution, requiring some physical processes to prevent the gas from cooling and eventually forming stars (e.g., McNamara & Nulsen 2007; Johansson et al. 2009; Conroy et al. 2015). While feedback powered by central supermassive black holes is frequently invoked as an explanation (e.g., McNamara & Nulsen 2007), observationally it has been difficult to directly connect active galactic nuclei activity to the quenching of star formation. Alternatively, the stars themselves may be crucial in providing additional heating, which is consistent with the observed anticorrelation between stellar surface density and specific star formation rate in both low- and high-redshift galaxies (e.g., Kauffmann et al. 2003, 2006; Franx et al. 2008; Fang et al. 2013; Whitaker et al. 2017). Specifically, it has been suggested that old stellar populations

can prevent continuing star formation in passive galaxies through energy injection from Type Ia supernovae (SNe Ia) and winds from asymptotic giant branch (AGB) stars (see Conroy et al. 2015 and references therein).

In a pilot study, Zahedy et al. (2016, hereafter Z16) employed high-resolution absorption-line spectroscopy of lensed background QSOs to examine the cool gas content in the inner halo ( $d = 3\text{--}15$  kpc) of three massive quiescent lensing galaxies at  $z = 0.4\text{--}0.7$ . While the gas content varied significantly among lenses and different sightlines of the same lens, a supersolar Fe/Mg relative abundance pattern,  $[\text{Fe}/\text{Mg}] \gtrsim 0.1$ , was found in every sightline where cool gas was detected ( $\sim 40\%$  of all sightlines). Such high  $[\text{Fe}/\text{Mg}]$  ratios indicate a significant contribution ( $\gtrsim 20\%$ ) from SNe Ia to the chemical enrichment history of the gas, exceeding what have been observed in mature stellar populations such as the solar neighborhood (e.g., Tsujimoto et al. 1995). Z16 suggest that these absorbers reside in the interstellar medium (ISM), where the gas is likely to have been enriched and heated by SNe Ia ejecta. However, to facilitate a direct comparison with different chemical enrichment models, it is necessary to probe the bulk of the cool ISM, neutral hydrogen (H I), and constrain its column density,  $N(\text{H I})$ .

We have obtained UV absorption spectra of the doubly lensed QSO HE 0047–1756 at  $z_{\text{QSO}} = 1.676$ , using the Space Telescope Imaging Spectrograph (STIS) on board the *Hubble Space Telescope* (*HST*). The lens of HE 0047–1756 at  $z = 0.408$  is a massive elliptical galaxy with a total stellar mass of  $M_{\star} \approx 10^{11} M_{\odot}$  and no ongoing star formation (Z16). Ultra-strong Mg II absorbers of rest-frame absorption equivalent width  $W_r(2796) > 3.6 \text{ \AA}$  are found along both lensed QSO sightlines probing opposite sides of this LRG lens at

$d = 4.6$  kpc (1.8 half-light radii,  $r_e$ ) and  $d = 3.3$  kpc (1.3  $r_e$ ). The STIS spectra allow us to measure the total integrated  $N(\text{H I})$  at two locations separated by  $\approx 8$  kpc in this massive quiescent galaxy, thereby constraining the mean gas metallicity. In this Letter, we report a large column density of extended neutral hydrogen gas detected in the inner ISM of the HE 0047–1756 lens, the first such discovery in a quiescent galaxy beyond  $z \sim 0$ . Throughout this Letter, we adopt a flat cosmology of  $\Omega_M = 0.3$  and  $\Omega_\Lambda = 0.7$ , with a Hubble constant of  $H_0 = 70 \text{ km s}^{-1} \text{ Mpc}^{-1}$ .

## 2. Observations and Data Reduction

Long-slit FUV spectroscopy of the doubly lensed QSO HE 0047–1756 was obtained on 2016 December 5 using the FUV-MAMA detector in *HST*/STIS with the  $52'' \times 0''.2$  long slit and the low-resolution G140L grating (PID: 14751; PI: Zahedy). This configuration provides a dispersion of  $\approx 0.6 \text{ \AA}$  per pixel with a corresponding spectral resolution of  $\approx 270 \text{ km s}^{-1}$ . Because the two lensed images of HE 0047–1756 are separated by merely  $1''.4$ , the long-slit spectroscopic mode of STIS enabled observation of both QSO images in a single setup, which was achieved by orienting the slit at a position angle of  $-9^\circ.51$ . At the redshift of the lensing galaxy, the broad wavelength coverage of the G140L grating (1150–1720  $\text{\AA}$ ) includes the entire H I Lyman series. The total integration time of the observations was 7689 s, which was divided into six individual exposures of roughly equal durations.

Individual spectral images were initially processed using the automatic STIS calibration pipeline, CALSTIS (Hodge et al. 1998), which performed dark and bias subtractions, flat-fielding, and wavelength calibration, and produced a series of data products including a two-dimensional rectified spectral image for each science exposure. The pipeline-calibrated data products were retrieved from the *HST* archive for further processing. We developed a custom spectral extraction software to optimize signal-to-noise ratio (S/N) in the resulting spectra, especially that of the fainter lensed QSO image HE 0047–1756B. The custom software first constructed a model spatial profile along the cross dispersion direction for each QSO image by averaging the two-dimensional rectified spectral image along the wavelength direction. Regions affected by strong sky emission lines were excluded from this exercise. Next, the software extracted individual QSO spectra by applying the mean spatial profile of each QSO image as optimal weights for the spatially resolved spectral signal at each wavelength. Finally, the optimally extracted one-dimensional spectra from individual exposures were coadded to form a single combined spectrum per QSO image, which is characterized by a mean S/N  $\approx 20$ –25 per resolution element for HE 0047–1756A, and S/N  $\approx 10$ –13 per resolution element for HE 0047–1756B, over the full wavelength range (1150–1720  $\text{\AA}$ ).

## 3. Large Interstellar $N(\text{H I})$ in the Massive Quiescent Lens

The final coadded FUV spectra of the two lensed QSO images are presented in Figure 1. The absorption features along sightline B (black) are redshifted by  $\approx 1.8 \text{ \AA}$  relative to those along sightline A (red), consistent with the kinematic offset of  $\approx 360 \text{ km s}^{-1}$  seen in Mg II, Fe II, and Mg I. Strong absorption features are detected along both sightlines, which can be

attributed to the H I Lyman series as well as various low- to high-ionization metal transitions at the redshift of the lensing galaxy.

For both sightlines, the FUV spectra exhibit a lack of continuum flux blueward of the Lyman limit (at  $\approx 1280 \text{ \AA}$  in observed wavelength) expected for the lens galaxy. The mean flux averaged over a finite spectral window below the Lyman limit is consistent with zero to within the  $1\sigma$  associated uncertainty, indicating that the absorbing gas at  $d \sim r_e$  from the lens galaxy of HE 0047–1756 is optically thick to hydrogen-ionizing photons. We estimate a  $2\sigma$  upper limit to the Lyman-continuum flux using the mean value of the error spectrum between 870 and 900  $\text{\AA}$  in the rest frame of the lens galaxy, which we then convert to a  $2\sigma$  lower limit to the continuum opacity by calculating its ratio to the mean continuum level redward of the Lyman limit at rest-frame 955–965  $\text{\AA}$ . Given that the H I photoionization cross-section varies as  $\sigma(\lambda) = 6.30 \times 10^{-18} (911.8 \text{ \AA}/\lambda)^{-3} \text{ cm}^2$  (Osterbrock & Ferland 2006), we estimate  $2\sigma$  lower limits of  $\log N(\text{H I}) > 17.8$  for HE 0047–1756A and  $\log N(\text{H I}) > 17.6$  for HE 0047–1756B at the lens redshift.

Including the entire Lyman series lines allows us to better constrain  $N(\text{H I})$ . We perform a Voigt-profile analysis using a custom program previously developed by and described in Z16. For each sightline, the combined spectrum is first continuum normalized using a low-order polynomial function. Then, a simultaneous Voigt-profile fit is performed on the following Lyman series lines: Ly $\alpha$   $\lambda 1215$ , Ly $\beta$   $\lambda 1025$ , Ly $\gamma$   $\lambda 972$ , Ly $\epsilon$   $\lambda 937$ , and Ly $\zeta$   $\lambda 930$ . The Ly $\delta$   $\lambda 949$  line is excluded from the fit because it is blended with the Galactic C II  $\lambda 1334$  absorption. Higher-order Lyman series lines (Ly-7 and onward) are also excluded due to contaminations by the [O I]  $\lambda\lambda 1302, 1306$  airglow emission-line doublet.

The Voigt-profile analysis results in a best-fit  $\log N(\text{H I}) = 19.7 \pm 0.1$  for the absorber along HE 0047–1756A and  $\log N(\text{H I}) = 19.6_{-0.3}^{+0.2}$  for the absorber along HE 0047–1756B. The quoted uncertainties represent the estimated 95% confidence level of the best-fit  $\log N(\text{H I})$ , marginalized over the Doppler parameter  $b$ . The best-fit Voigt profiles of the Lyman series lines are presented in Figure 2 (in red) along with the data (in black). A lower  $N(\text{H I})$  value fails to reproduce the damping wing of the Ly $\alpha$  line, demonstrating that strong constraints can be obtained for  $N(\text{H I})$  based on the low-resolution STIS spectra. We also perform a curve-of-growth (COG) analysis for estimating  $N(\text{H I})$  along each sightline and find consistent results with the Voigt-profile analysis, with  $\log N(\text{H I}) = 19.6 \pm 0.2$  for A and  $\log N(\text{H I}) = 19.5_{-0.4}^{+0.2}$  for B, and an effective  $b$  value of  $135 \pm 10 \text{ km s}^{-1}$  for A and  $125 \pm 15 \text{ km s}^{-1}$  for B. The large effective  $b$  values are understood to be driven by gas kinematics rather than the actual thermal width of the gas. To quantify the uncertainties in  $N(\text{H I})$  and  $b$  as a result of uncertainties in the STIS line-spread function (LSF), we repeat the Voigt-profile analysis by varying the width of the STIS LSF, and find that a 10% change in the LSF results in less than a 5% change in the best-fit  $b$  and less than a 10% change in  $N(\text{H I})$ .

## 4. Discussion and Implications

Our analysis of the STIS spectra of the doubly lensed QSO HE 0047–1756 has yielded, for the first time, constraints on the neutral gas content at two locations separated by  $\approx 8$  kpc in a massive quiescent galaxy beyond  $z \sim 0$ . The range of observed

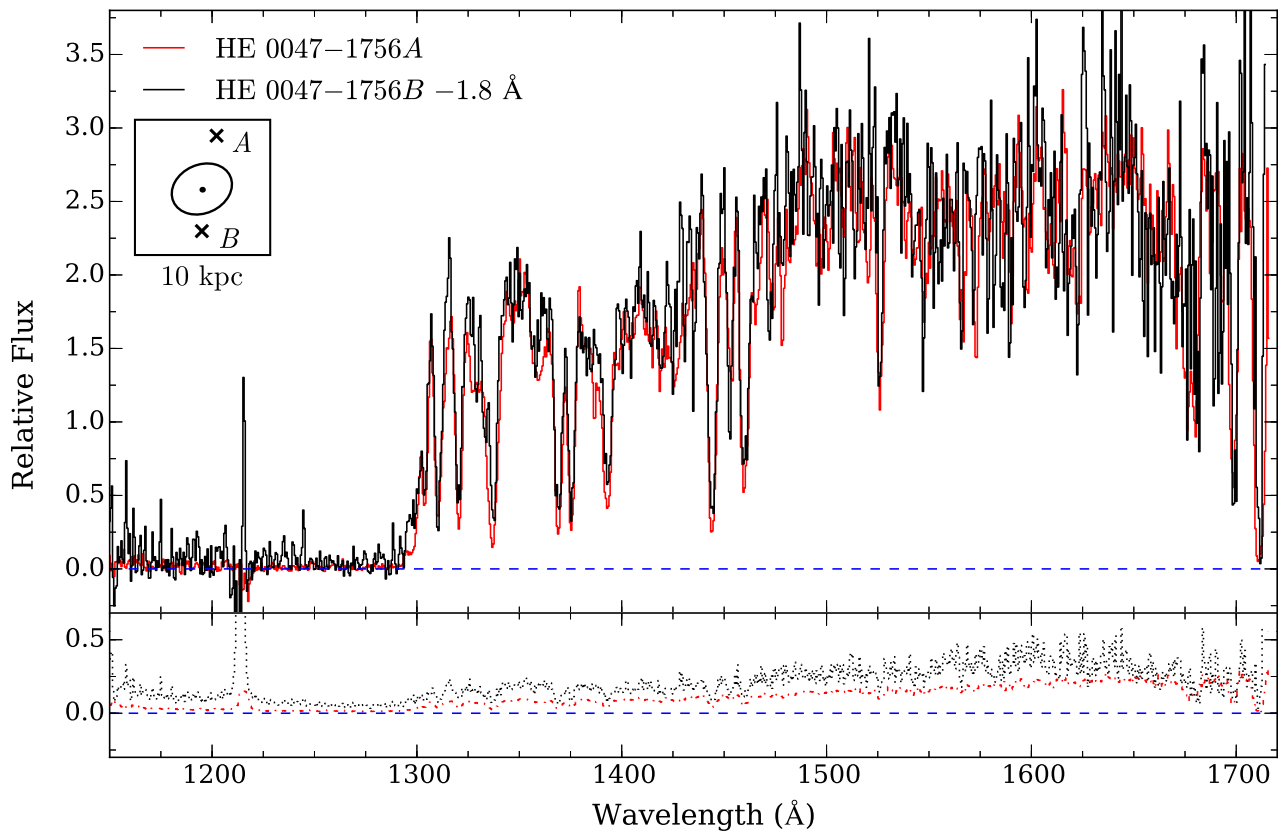


**Figure 1.** *HST/STIS* FUV spectra of the doubly lensed QSO HE 0047–1756. The spectrum of HE 0047–1756B (red) has been shifted blueward by 1.8 Å to align the absorption features with those seen in HE 0047–1756A (black). The corresponding  $1\sigma$  error spectra are shown as dotted lines in the bottom panel. The zero flux level is indicated with the blue dashed line. Inset: the configuration of the two lensed QSO sightlines (shown with crosses) in a  $10 \times 10$  kpc region around the lensing galaxy (shown with an ellipse). The size and orientation of the ellipse correspond to the half-right radius and position angle of the semimajor axis of the lens galaxy as described in Z16.

$N(\text{H I})$  along both lensed sightlines,  $\log N(\text{H I}) = 19.6\text{--}19.7$ , is comparable to what is commonly seen in 21 cm maps of the ISM in nearby early-type galaxies ( $\log N(\text{H I}) \approx 19.3\text{--}20.3$ ; e.g., Oosterloo et al. 2010; Serra et al. 2012), but is high among previous single-sightline surveys of more distant passive galaxies (e.g., Thom et al. 2012; Prochaska et al. 2017). Detections of high- $N(\text{H I})$  absorbers at two different locations suggest the presence of extended interstellar H I. Here, we discuss the implications of this finding.

#### 4.1. Chemical Enrichment Level in the Cool ISM of the Lens

While the detailed gas kinematics are not resolved in the low-resolution spectra, the line centroids can be determined to high accuracy. The H I gas kinematics are found to match well with the kinematics of the Fe II absorption complex revealed in ground-based echelle data. Both H I and metal absorption lines display a large velocity shear of  $v_B - v_A = +360 \text{ km s}^{-1}$  over a projected distance of  $\approx 8$  kpc across the quiescent galaxy, flanking the systemic redshift of the lens.

We estimate a mean gas metallicity averaged across all components by combining the newly available  $N(\text{H I})$  and previously published total Fe II column densities from Zahedy et al. (2017). The Fe abundance of the gas,  $(\text{Fe}/\text{H})$ , is related to the observed column density ratio of Fe II and H I corrected for the expected ionization fractions, following  $\log(\text{Fe}/\text{H}) = \log N(\text{Fe II})/N(\text{H I}) - \log(f_{\text{Fe}^+}/f_{\text{H}^0})$ . In the absence of a large relative ionization fraction correction, with  $\log(f_{\text{Fe}^+}/f_{\text{H}^0}) \sim 0$ ,

the observed column density ratio translates directly into the Fe abundance,  $\log N(\text{Fe II})/N(\text{H I}) \approx \log(\text{Fe}/\text{H})$ .

We perform a series of photoionization calculations using CLOUDY v.13.03 (Ferland et al. 2013) to estimate the necessary ionization fraction corrections for a wide range of gas densities and metallicities in a photoionized gas of temperature  $T = 10^4$  K and  $\log N(\text{H I}) = 19.6\text{--}19.7$ . We assume a plane-parallel slab, illuminated on both sides with the updated Haardt & Madau (2001) ionizing background radiation field (HM05 in CLOUDY) at  $z = 0.4$ . Adopting a maximum cloud size leads to a lower limit on the allowed gas density for a given  $N(\text{H I})$ . We adopt a maximum cloud size of 1 kpc, consistent with observations of Galactic high-velocity clouds (e.g., Putman et al. 2012) and find  $n_{\text{H}} \gtrsim 10^{-1.6} \text{ cm}^{-3}$  for the absorbers along the two lensed QSO sightlines. Over this allowed gas density range, the calculations show that the gas is mostly neutral with  $f_{\text{H}^0} > 0.6$  and the relative ionization fraction correction between  $\text{Fe}^+$  and  $\text{H}^0$  is  $(f_{\text{Fe}^+}/f_{\text{H}^0}) \approx 1$ . Therefore, to a good approximation, the gas metallicity can be estimated directly from  $\log N(\text{Fe II})/N(\text{H I})$ , following  $[\text{Fe}/\text{H}] \approx \log N(\text{Fe II})/N(\text{H I}) - \log(\text{Fe}/\text{H})_{\odot}$ .<sup>5</sup>

The total Fe II column density is  $\log N(\text{Fe II}) = 14.61 \pm 0.02$  for the absorber along HE 0047–1756A and  $\log N(\text{Fe II}) = 14.70 \pm 0.08$  for the absorber along HE 0047

<sup>5</sup> If the intrinsic  $N(\text{H I})$  of the Fe II absorbing gas is lower than observed (namely, only part of the observed  $N(\text{H I})$  is cospatial with the Fe II gas), then the gas metallicity would be higher still.

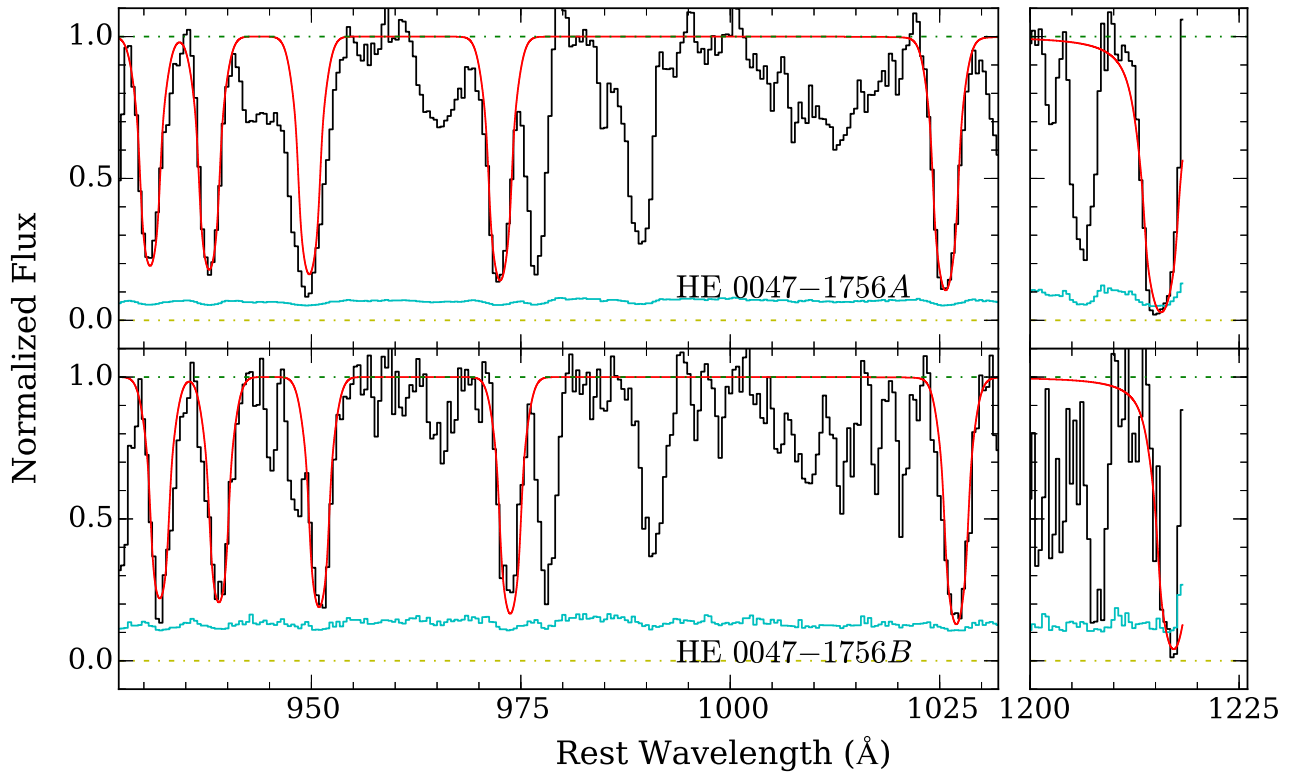


**Figure 2.** Continuum-normalized absorption profile of H I Lyman series transitions along the doubly lensed QSO sightlines HE 0047–1756A (top) at  $d = 4.6$  kpc (or  $1.8 r_e$ ) and HE 0047–1756B (bottom) at  $d = 3.3$  kpc (or  $1.3 r_e$ ) from the HE 0047–1756 lens galaxy. The  $x$ -axis corresponds to the rest-frame wavelength of the galaxy at  $z = 0.408$ . The  $1\sigma$  error spectra are plotted in cyan histograms. The best-fit Voigt-profile models for the H I Lyman series, convolved with the STIS LSF, are included in red, with  $\log N(\text{H I}) = 19.7_{-0.1}^{+0.1}$  for the absorber along HE 0047–1756A and  $\log N(\text{H I}) = 19.6_{-0.3}^{+0.2}$  for the absorber along HE 0047–1756B. Note that the Ly $\delta$   $\lambda 949$  line is contaminated by C II  $\lambda 1334$  absorption from the Milky Way ISM.

–1756B (Z16; Zahedy et al. 2017). Adopting the solar chemical abundance pattern from Asplund et al. (2009), where  $\log(\text{Fe}/\text{H})_{\odot} = -4.50 \pm 0.04$ , we find that the estimated Fe abundance is  $[\text{Fe}/\text{H}] = -0.6 \pm 0.1$  for the absorber along HE 0047–1756A, and  $[\text{Fe}/\text{H}] = -0.4 \pm 0.3$  for the absorber along HE 0047–1756B.

#### 4.2. Effects of Dust Depletion

Dust depletion, when unaccounted for, can lead to underestimated chemical abundances, particularly in high-metallicity gas. For the HE 0047–1756 lens, Ca II  $\lambda\lambda$  3934,3969 absorption has also been observed along both sightlines (Z16). It has been shown that the strength of Ca II absorption correlates with both reddening (Murga et al. 2015) and the [Cr/Zn] relative abundance (e.g., Zych et al. 2009), two common diagnostics of the dust content. Z16 previously reported  $W_r(3934) = 0.3 \text{ \AA}$  and  $W_r(3934) = 0.1 \text{ \AA}$  for the absorption systems along sightlines A and B, respectively. For moderately strong Ca II absorbers of  $W_r(3934) = 0.1\text{--}0.5 \text{ \AA}$ , the range of observed [Cr/Zn] is  $[\text{Cr}/\text{Zn}] \sim -0.4 \pm 0.2$  (e.g., Zych et al. 2009 and references therein). The inferred [Cr/Zn] level indicates a modest amount of dust depletion similar to that seen in the Galactic halo, where the expected amount of Fe depletion is 0.5–0.6 dex (e.g., Savage & Sembach 1996; De Cia et al. 2016). For both sightlines, applying the expected dust depletion leads to still higher gas metallicities, reaching solar or supersolar values,  $[\text{Fe}/\text{H}] \gtrsim 0$ , and comparable to the typical mean metallicities in the hot ISM of nearby ellipticals,

$[\text{Fe}/\text{H}] \gtrsim 0\text{--}0.3$  (e.g., Humphrey & Buote 2006; Loewenstein & Davis 2010, 2012).

#### 4.3. Fe Mass Budget

In Z16, we reported a supersolar [Fe/Mg] abundance pattern in the lensing galaxy and suggested that the gas has been enriched by the Fe-rich ejecta from SNe Ia. Now that we have estimated the gas metallicity, we can estimate the total Fe mass observed in the cool ISM and compare it with the expected contribution from SNe Ia.

The Fe mass in the cool ISM of the lens is estimated based on the observed  $N(\text{H I})$ , the inferred solar gas metallicity, and the ionization state of the gas from the CLOUDY models in Section 4.1. We find a total Fe mass within  $d = 5$  kpc ( $\approx 2 r_e$ ; the region probed by the doubly lensed QSO) of  $M_{\text{cool}}(\text{Fe}) \sim (5\text{--}8) \times 10^4 (f_{\text{cov}}) M_{\odot}$  in the cool ISM of the lens, where  $f_{\text{cov}}$  is the cool gas covering fraction.

Next, we estimate the expected SNe Ia contribution based on the observed rate and expected yields of SNe Ia. The observed radial distribution of SNe Ia in elliptical galaxies follows the stellar light distribution (Förster & Schawinski 2008). The mean SNe Ia rate per unit stellar mass is found to be 0.044 SNe per century per  $10^{10} M_{\odot}$  in nearby ellipticals (Mannucci et al. 2005). Combining these findings, we estimate that the integrated SNe Ia rate within  $d \sim 5$  kpc of the lens is  $\sim 0.3$  per century. Given a minimum stellar population age of  $\approx 1$  Gyr for this galaxy (Z16) and assuming a constant SNe Ia rate, a total of  $3 \times 10^6$  SNe Ia should have occurred in this volume. Because SN Ia is expected to produce  $\approx 0.6\text{--}0.7 M_{\odot}$  in

Fe (e.g., Iwamoto et al. 1999), the estimated total number of SNe Ia leads to an expected total Fe mass of  $M_{\text{FeIa}} \sim 2 \times 10^6 M_{\odot}$  over the 1 Gyr time interval. Note that if the SNe Ia rate were higher in the past, then this estimate should be considered as a lower limit. Comparing  $M_{\text{cool}}(\text{Fe})$  to  $M_{\text{FeIa}}$ , we conclude that the Fe uncovered in the absorbers accounts for at most  $\sim 5\%$  of all Fe produced by SNe Ia over the lifetime of a massive elliptical galaxy. As a result, the majority of Fe must reside in a hot ISM phase.

Although no direct observations of the hot ISM are available for this quiescent galaxy, we could use nearby massive ellipticals as a reference. X-ray observations have shown that their hot ISM has a typical mean  $[\text{Fe}/\text{H}] \sim 0$  and a mean central density of  $n_{\text{H}} \sim 0.1 \text{ cm}^{-3}$  (e.g., Mathews & Brighenti 2003). Adopting these numbers, we infer a total hot-phase Fe mass within  $2 r_c$  of  $M_{\text{hot}}(\text{Fe}) \sim 2.5 \times 10^6 M_{\odot}$ , in good agreement with the expected contribution from SNe Ia. Therefore, the implication that the majority of Fe produced in SNe Ia resides in the hot phase is at least consistent with the empirical understanding of nearby massive ellipticals.

### 5. Conclusions

Using *HST*/STIS UV spectra of the doubly lensed images of QSO HE 0047–1756, we have discovered a high column density of neutral hydrogen gas at  $3 < d < 5$  kpc (or  $r_c < d < 2 r_c$ ) from a massive ( $M_{\text{star}} \approx 10^{11} M_{\odot}$ ) elliptical lens galaxy at  $z = 0.408$ . The new STIS spectra not only allow direct measurements of the ISM  $N(\text{HI})$  and metallicity, but also constrain the Fe mass budget in this distant elliptical. We find an ISM  $N(\text{HI})$  of  $\log N(\text{HI}) = 19.6\text{--}19.7$  at two locations separated by  $\approx 8$  kpc on opposite sides of the galaxy. This large  $N(\text{HI})$  is comparable to the range of  $N(\text{HI})$  in nearby ellipticals. The Fe abundance is 0.3–0.4 solar along both sightlines, which increases to solar or supersolar after accounting for likely dust depletions. Together, the observed  $N(\text{HI})$  and Fe abundance constrain the Fe mass budget. For a 100% gas covering fraction, we infer a total Fe mass of  $M_{\text{cool}}(\text{Fe}) \sim (5\text{--}8) \times 10^4 M_{\odot}$  in the cool ISM of the lens. Including previous findings that SNe Ia contribute significantly to the chemical enrichment in massive quiescent halos (e.g., Mernier et al. 2017), we find that the majority ( $\approx 95\%$ ) of Fe produced by SNe Ia resides in the hot phase. Future studies probing warm ( $T \sim 10^{5-6}$  K) gas in the halos of luminous red galaxies using high-ionization metal absorption (e.g., O VI, likely tracing cooling gas) will provide new insights into SNe Ia heating and assess its relative importance to other forms of late-time feedback in the halos of massive quiescent galaxies.

We thank Annalisa de Cia, Sean Johnson, and John Mulchaey for helpful discussions. F.S.Z. and H.W.C. acknowledge partial support from HST-GO-14751.01A. F.S.Z. acknowledges support from the Brinson Foundation predoctoral fellowship. A.I.Z. acknowledges support from NSF grant AST-1211874. This work is based on data gathered with the NASA/ESA *Hubble Space Telescope* operated by the Space

Telescope Science Institute and the Association of Universities for Research in Astronomy, Inc., under NASA contract NAS 5-26555.

### ORCID iDs

Fakhri S. Zahedy  <https://orcid.org/0000-0001-7869-2551>  
 Hsiao-Wen Chen  <https://orcid.org/0000-0001-8813-4182>  
 Ann Zabludoff  <https://orcid.org/0000-0001-6047-8469>

### References

- Asplund, M., Grevesse, N., Sauval, A. J., & Scott, P. 2009, *ARA&A*, 47, 481  
 Bergeron, J., & Stasińska, G. 1986, *A&A*, 169, 1  
 Bowen, D. V., & Chelouche, D. 2011, *ApJ*, 727, 47  
 Conroy, C., van Dokkum, P. G., & Kravtsov, A. 2015, *ApJ*, 803, 77  
 De Cia, A., Ledoux, C., Mattsson, L., et al. 2016, *A&A*, 596, A97  
 Fang, J. J., Faber, S. M., Koo, D. C., & Dekel, A. 2013, *ApJ*, 776, 63  
 Ferland, G. J., Porter, R. L., van Hoof, P. A. M., et al. 2013, *RMxAA*, 49, 137  
 Förster, F., & Schawinski, K. 2008, *MNRAS*, 388, L74  
 Franx, M., van Dokkum, P. G., Förster Schreiber, N. M., et al. 2008, *ApJ*, 688, 770  
 Gauthier, J.-R., Chen, H.-W., & Tinker, J. L. 2009, *ApJ*, 702, 50  
 Gauthier, J.-R., Chen, H.-W., & Tinker, J. L. 2010, *ApJ*, 716, 1263  
 Grossi, M., di Serego Alighieri, S., Giovanardi, C., et al. 2009, *A&A*, 498, 407  
 Haardt, F., & Madau, P. 2001, in *Clusters of Galaxies and the High Redshift Universe Observed in X-rays*, ed. D. M. Neumann & J. T. T. Van (Saclay: CEA), 64  
 Hodge, P., Baum, S., McGrath, M., et al. 1998, *Calstis0: Pipeline Calibration of STIS Data—A Detailed View*, Instrum. Sci. Rep. STIS 98-10 (Baltimore, MD: STScI), <http://adsabs.harvard.edu/abs/1998stis.rept...10H>  
 Huang, Y.-H., Chen, H.-W., Johnson, S. D., & Weiner, B. J. 2016, *MNRAS*, 455, 1713  
 Humphrey, P. J., & Buote, D. A. 2006, *ApJ*, 639, 136  
 Iwamoto, K., Brachwitz, F., Nomoto, K., et al. 1999, *ApJS*, 125, 439  
 Johansson, P. H., Naab, T., & Ostriker, J. P. 2009, *ApJL*, 697, L38  
 Kauffmann, G., Heckman, T. M., De Lucia, G., et al. 2006, *MNRAS*, 367, 1394  
 Kauffmann, G., Heckman, T. M., White, S. D. M., et al. 2003, *MNRAS*, 341, 54  
 Loewenstein, M., & Davis, D. S. 2010, *ApJ*, 716, 384  
 Loewenstein, M., & Davis, D. S. 2012, *ApJ*, 757, 121  
 Mannucci, F., Della Valle, M., Panagia, N., et al. 2005, *A&A*, 433, 807  
 Mathews, W. G., & Brighenti, F. 2003, *ARA&A*, 41, 191  
 McNamara, B. R., & Nulsen, P. E. J. 2007, *ARA&A*, 45, 117  
 Mernier, F., de Plaa, J., Kaastra, J. S., et al. 2017, *A&A*, 603, A80  
 Murga, M., Zhu, G., Ménard, B., & Lan, T.-W. 2015, *MNRAS*, 452, 511  
 Oosterloo, T., Morganti, R., Crocker, A., et al. 2010, *MNRAS*, 409, 500  
 Osterbrock, D. E., & Ferland, G. J. 2006, *Astrophysics of Gaseous Nebulae and Active Galactic Nuclei* (2nd ed.; Sausalito, CA: Univ. Science Books)  
 Prochaska, J. X., Werk, J. K., Worseck, G., et al. 2017, *ApJ*, 837, 169  
 Putman, M. E., Peek, J. E. G., & Joung, M. R. 2012, *ARA&A*, 50, 491  
 Savage, B. D., & Sembach, K. R. 1996, *ARA&A*, 34, 279  
 Serra, P., Oosterloo, T., Morganti, R., et al. 2012, *MNRAS*, 422, 1835  
 Thom, C., Tumlinson, J., Werk, J. K., et al. 2012, *ApJL*, 758, L41  
 Tsujimoto, T., Nomoto, K., Yoshii, Y., et al. 1995, *MNRAS*, 277, 945  
 Whitaker, K. E., Bezanson, R., van Dokkum, P. G., et al. 2017, *ApJ*, 838, 19  
 Young, L. M., Scott, N., Serra, P., et al. 2014, *MNRAS*, 444, 3408  
 Zahedy, F. S., Chen, H.-W., Gauthier, J.-R., & Rauch, M. 2017, *MNRAS*, 466, 1071  
 Zahedy, F. S., Chen, H.-W., Rauch, M., Wilson, M. L., & Zabludoff, A. 2016, *MNRAS*, 458, 2423  
 Zych, B. J., Murphy, M. T., Hewett, P. C., & Prochaska, J. X. 2009, *MNRAS*, 392, 1429